The source regions and storm-effectiveness of frontside full halo coronal mass ejections

X. P. Zhao
W. W. Hansen Experimental Physics Laboratory, Stanford University, USA

D. F. Webb
ISR, Boston College, Chestnut Hill, MA, USA

Short title: FRONTSIDE FULL HALO CORONAL MASS EJECTIONS

Abstract. Full halo coronal mass ejections (CMEs) erupting from the side of the Sun facing Earth, i.e., frontside full halo CMEs, are considered to be the most likely source of geomagnetic storms. However, this hypothesis has not been tested over a full solar cycle. We compare all frontside full halo CMEs observed during the first half of solar cycle 23, from 1996 to the end of 2000, with moderate or larger storms at Earth. We show that the association of frontside full halo CMEs with such storms tends to decrease from 1997 to 2000, though this decreasing trend is not monotonic. We examine the locations of the frontside full halo CMEs from 1996 to 2000 with respect to two kinds of coronal closed field regions: bipolar closed field regions between opposite-polarity open field regions and unipolar closed field regions between like-polarity open field regions. We find that even during solar maximum when the occurrence frequency of the two kinds of regions is nearly the same, the central positions of the frontside full halo CMEs are mostly located under the bipolar coronal streamer belt, suggesting that most full halo CMEs originate in the bipolar coronal helmet streamers that are sandwiched between coronal holes having opposite magnetic polarity. Because the inclination of the heliospheric current sheet increases towards solar maximum, the fraction of CMEs emitted into the ecliptic decreases and the inclination of associated flux ropes increases. These effects help to explain the solar cycle effect on the storm-effectiveness of frontside full halo CMEs.

1. Introduction

Coronal mass ejections (CMEs) are now known to be a key causal link among solar eruptions, major interplanetary disturbances and geomagnetic storms (Gosling et al., 1991; Kahler, 1992; Webb et al., 2001). But CMEs thought to originate near the solar limb are less likely to strike the Earth and, therefore, to drive geomagnetic storms. Halo CMEs, those which appear as expanding, circular brightenings that completely surround a coronagraph's occulting disk, are now being routinely observed by the SOHO LASCO coronagraphs (Brueckner et al., 1995). Their observation suggests that these CMEs represent a broad shell or bubble of dense plasma propagating radially toward (or away from) the Earth from the sources near the center of the solar disk (Howard et al., 1982; St. Cyr et al., 2000; Webb et al., 2000). LASCO has detected halo CMEs during the ascending and maximum phases of this cycle at about 10% the rate of all CMEs (Webb, 2002). This rate includes partial halo CMEs, often defined as those with spans $\geq$140°. Halo CMEs are of clear importance to space weather research because such events, especially when associated with visible solar activity, imply the launch of a disturbance aimed towards Earth. These so-called "frontside" halo CMEs, especially those exhibiting a full halo completely surrounding the occulting disk, may directly strike Earth and, therefore, potentially cause geomagnetic storms. In what follows we call the frontside full halo CME, the FFH CME.

Webb et al. (2000) showed recently that all six frontside halo, full or partial, CMEs observed with source regions within a half solar radius from the geometric center of the solar disk by LASCO from December 1996 to June 1997 were associated with shocks, magnetic clouds, and moderate geomagnetic storms (i.e., peak Dst<-50 nT) at the Earth 3-5 days after leaving the Sun. Thus, all six of the events were storm-effective during this period of time. This observation suggests that shocks and magnetic cloud-like structures or magnetic flux ropes are common features of halo CMEs. However, after 1997 there were an increasing number of frontside halo CMEs that could not be associated with

geomagnetic storms. Does this difference in storm-effectiveness of frontside halo CMEs indicate the existence of a solar-cycle effect in the geoeffectiveness of CMEs? If so, what is the cause of this solar cycle effect? Despite their relatively low rate of occurrence, we have now observed a sufficient number of full halo CMEs to permit a statistically robust study of their characteristics and associations. Webb et al. [The Characteristics and Associations of Full Halo CMEs; Journal of Geophysical Research; in preparation, 2002] discusses the results of study of all 134 full halo LASCO CMEs observed from August 1996 to the end of 2000. In Section 2, we use some of these results to analyze the year-to-year variation in the storm-effectiveness of the 80 FFH CMEs. The yearly variation in the storm-effectiveness may be associated with a solar cycle evolution in the characteristics of the source regions of the FFH CMEs. The characteristics of the large-scale closed field regions that are the likely source regions of the FFH CMEs are examined from sunspot minimum to maximum in Section 3. The overall solar cycle evolution of the FFH CME source regions and of the FFH CMEs themselves are studied by mapping them onto synoptic maps of the photospheric magnetic field. In Section 4 we describe this plotting technique. Finally, the results are summarized and discussed in the last section.

2. Yearly variation of storm-effectiveness

During the 4.5-year period from the middle of 1996 to the end of 2000, the LASCO coronagraphs observed a total of 134 full halo CMEs (Webb et al., 2002). To identify which of the full halo CMEs were from the frontside, and to determine whether or not the FFH CMEs were storm-effective, the degree of association of each full halo event with near-surface solar activity, interplanetary disturbances and geomagnetic storms was determined. The criteria used to make these associations are described by Webb et al. (2000, 2001). The solar surface activity considered to be associated with CMEs includes flares and disappearing filaments in H_α observations, long-duration flares,

post-eruption arcade formation, depletions or 'dimmings' of the coronal intensity, and bright wavefronts propagating quasi-radially from the source region in EUV observations (Thompson et al., 1998). The signatures of CME-associated interplanetary disturbances (ICMEs) include transient interplanetary shocks, bidirectional streaming of electrons and protons, magnetic clouds and other signatures of ejecta (e.g., Neugebauer and Goldstein, 1997; Cane et al., 2000). The solar wind observations were primarily from the Wind spacecraft with additional data from ACE after its operations began in August 1997.

Table 1. Storm-effectiveness of Frontside Full Halo (FFH) CMEs

Year (Number of Observational Days)	1996 (150)	1997 (365)	1998 (240)	1999 (274)	2000 (343)	1996-2000 (1372)
Annual Mean Sunspot Number	8.6	21.5	64.3	93.2	119.6	
Full Halo CMEs	3	18	23	27	63	134
All FFH CMEs	0	11	13(2)	13(2)	33(6)	70(10)
Storm-associated All FFH CMEs	0	10	7	5	23	45
Fraction		0.91	0.54	0.38	0.70	0.64
Centered FFH CMEs	0	8	7(2)	9(2)	25(6)	49(10)
Storm-associated Center FFH CMEs	0	8	5	4	18	35
Fraction		1.00	0.71	0.44	0.72	0.71

Of the 134 full halo CMEs, Webb et al. (2002) estimate that the source regions of 80 of them were located on the frontside of the Sun, and, hence, could be aimed Earthward. Table 1 presents the annual distribution of the FFH CMEs and their storm associations. We used the same definition of a geomagnetic storm as Webb et al. (2000): an extended period of geomagnetic activity having a peak Dst<-50 nT. To be associated with the halo CME, this activity had to occur at the Earth within 5 days of CME onset. The second and third rows in Table 1 list the annual numbers of sunspots and of all full halo CMEs, both frontside and backside. The mean sunspot numbers are from Solar Geophysical Data Bulletins (2002) and indicate that sunspot (activity)

minimum occurred in 1996 and maximum in 2000 (a secondary peak also occurred in 2001.) Thus, our data cover the complete ascending phase and maximum of this cycle. The 4th and 5th rows list the annual numbers of the FFH CMEs and the subset which are associated with storms. Among 80 FFH CMEs there were 10 that occurred too close together in time to distinguish separate storms at Earth. These 10 events were excluded from the fractional associations. The numbers in parentheses in the 4th and 7th rows show the annual numbers of the "too close" CMEs. The 6th row shows the fraction of the number of the storm-associated to the total number of FFH CMEs. All of these values are listed in columns by year from 1996 through 2000, with the totals in the last column. We add these caveats about the associations between the halo events and storms. As solar activity increases, it becomes more difficult to make unambiguous associations due to periods of frequent halo events and the increasing complexity of the solar wind. In addition, the annual number of full halo CMEs in 1996 is too small to get any statistical result with significance, and the annual numbers of FFH CMEs from 1997 to 2000 are small so that we can discuss only trends in these data. We note that the fractional association between FFH CMEs and storms decreased markedly as sunspot number increased from 0.9 in 1997 to 0.4 in 1999. It then increased again to 0.7 at maximum in 2000. As discussed in Sections 4 and 5, this increase may be, at least partially, associated with the clustering occurrence of FFH CMEs in fewer bipolar helmet streamers that are good for generating storm-effective CMEs, and the increasing complexity of the solar wind in 2000.

We might expect the geoeffectiveness of FFH CMEs to be dependent on the location of their associated surface activity; i.e., CMEs with source regions nearer the Sun's disk center would be more geoeffective (Webb et al., 2000; Cane et al., 2000). To examine this possible dependence, the fractional associations for the most "centered" FFH CMEs, i.e., those with their associated surface activity located within 45° of the geometrical center of the solar disk (i.e., the sub-Earth point), were analyzed separately.

The 7th to 9th rows of Table 1 list the annual numbers of the centered FFH CMEs, the subset which are associated with storms, and the fractional association. As expected, the fractional associations for centered FFH CMEs for all years were higher than the fractions for all FFH CMEs, especially for 1998.

3. Two kinds of large-scale closed field regions

The inferred year-to-year variation in the storm-effectiveness of FFH CMEs implies that factors other than the mere occurrence of a CME directed toward Earth are important in determining the level of geomagnetic activity. It has been shown that near the maximum of cycle 21 during 1978-1979 many fast CMEs that struck the magnetosphere did not produce intense storms, because they did not have sustained periods of strong southward field (Tsurutani et al., 1988). The storm-effective solar wind structures include long intervals of enhanced southward interplanetary magnetic field, or Bs "events" (e.g., Tsurutani and Gonzalez, 1997; Zhao et al., 1993). The variation of storm-effective solar wind structures that cause the year-to-year variation in the storm-effectiveness of FFH CMEs may be associated with the different characteristics of source regions of FFH CMEs in the different phases of solar activity.

CMEs are large-scale dynamic phenomena in the corona that are believed to originate in large-scale closed field regions having sufficient free magnetic energy to drive the CME material outward against the magnetic tension force of closed structures and solar gravity (Hundhausen, 1993; 1999). Many energetic CMEs actually involve the disruption ("blowout") of a preexisting streamer, which can increase in brightness and size for days before erupting as a CME (Howard et al., 1985; Hundhausen, 1993). The streamer usually disappears afterwards, but often eventually reforms (Zhao and Hoeksema, 1996).

Coronal helmet streamers observed in white light are assumed to be closed field regions. There are two kinds of magnetic field topologies that can exist underneath

helmet streamers, as was first sketched by Hundhausen (1972) in his Figure 7.1. One includes, typically, a single arcade, and the other two arcades. In what follows we call the former a 'bipolar' helmet streamer and the latter a 'unipolar' helmet streamer, depending on the magnetic field polarities at the outermost feet of the streamer. The bipolar helmet streamer occurs between coronal holes (open field regions) having opposite magnetic polarity, and sometimes includes three arcades (Schwenn et al., 1997; Webb et al., 1997). Near sunspot minimum nearly all the coronal holes are located in the polar regions. All helmet streamers occur between the northern and southern polar coronal holes with opposite magnetic polarity, and form the bipolar helmet streamer belt in the corona which is the base of the heliospheric current sheet. As sunspot number increases, coronal holes begin to appear at low latitudes as well as high latitudes. It would be expected that the occurrence rate for unipolar streamers sandwiched between like-polarity coronal holes would also increase as solar activity increases, possibly producing a unipolar coronal streamer belt (called 'chains of streamers' or 'streamer belt without a neutral line' by Eselevich et al., 1999) as well as the bipolar streamer belt. Apparent dual arcade/single helmet streamer structures have been observed at eclipses (e.g., Saito and Tandberg-Hanssen, 1973). Webb et al. (1997) noted that some of these structures could also be quadrupolar, i.e., having 3 bipoles under the streamer. Figure 1 is the sketch of the solar corona observed at the November 12, 1996 eclipse, which is copied from Figure 2 in Saito and Tandberg-Hanssen (1973). The twin arch (dual arcade) system and an overlying helmet streamer are seen in the NW quadrant.

It has been shown that coronal holes and the bipolar coronal streamer belt can be reproduced as the foot points of open field lines and the magnetic neutral line using Carrington synoptic charts of the photospheric magnetic field and the potential field-source surface model (e.g. Zhao et al., 1999). Figure 2 displays observed coronal holes and active regions in 10830$\AA$ and the computed coronal open and closed field regions for Carrington rotation 1911 and 1935, showing the extent to which computed

open field regions agree with observed coronal holes, and showing that more low-latitude holes occurred in the ascending phase than in the minimum phase. The large white and black areas in the 10830$\mathring{A}$ maps (panels 1 and 3 from the top) are coronal holes and active regions, respectively. The blue and red dot areas in the coronal field maps (panels 2 and 4 from the top) denote the foot points of open field lines directed away from and toward the Sun. The lines consisting of blue (upward) and red (downward) segments denote all closed field lines with their apices located below 1.25 solar radii. The green (black) line in panels 1 and 3 (2 and 4) is the magnetic neutral line on the source surface at 2.5 solar radii where Br=0. As shown in panels 1 and 2 near sunspot minimum, most closed field regions are sandwiched between the opposite-polarity polar holes, and contain odd number bipoles. In the ascending phase of solar activity in panels 3 and 4, in addition to the bipolar closed field regions underneath the neutral line that contain one or three bipoles, as pointed to by purple arrows, there are unipolar closed field regions pointed to by green arrows. The unipolar closed field region is that which is sandwiched between like-polarity open field regions and is located far from the neutral line. As shown by the two closed field regions (green arrows) in Panel 4, the unipolar closed field region contains an even number of bipoles. Panel 3 indicates that in addition to the active regions (black areas) under the neutral line, there are two black areas pointed to by two green arrows that are located far away from the neutral line and corresponding to the unipolar large-scale closed field regions in panel 4. These two active regions can also be identified in the EIT synoptic maps for CR1935. In Mauna Loa and LASCO white-light synoptic maps for CR1935 (not shown here), however, there is only a thin bright feature corresponding to the unipolar closed field region near 360° longitude and +40° latitude; for the other unipolar region near 80° longitude no bright feature exists in the white-light synoptic maps because the two parallel magnetic arcades near 80° longitude align vertically so that the scattered white light in the line-of-sight from electrons within the unipolar closed field region is minimized (Wang

et al., 2000). Both Figures 1 and 2 show observationally unipolar magnetic closed field regions, though the existence of dense material in the corona and in the solar wind that might define the unipolar streamer and unipolar streamer belt is somewhat controversial (e.g., Eselevich, 1998).

Figure 3 shows open and closed field regions near sunspot maximum and the unipolar boundary layer as well as the bipolar boundary layer of open field regions at the source surface. The top panel of Figure 3 displays the distribution of the two kinds of closed field regions near sunspot maximum during CR 1961 (April 2000). There are eleven open field regions marked by different colors in the panel. The magnetic polarity of each open field region with a specified color may be found from the area with same color at the source surface in the bottom panel. Here symbols '+' and '−' denote the magnetic polarities away from and toward the Sun, respectively, as shown in the dark blue and purple holes. The closed field regions far from the neutral lines, for example, those between the red and green open field regions and between the green and dark blue open field regions, occur between like-polarity open field regions. The middle panel shows the radial variation of the boundary of the open field regions from 1.0 to 2.5 solar radii. The bottom panel shows the boundary layers of open field regions at 2.5 solar radii. In addition to the bipolar boundary layer between opposite-polarity open field regions, i.e., the magnetic neutral line aligned with the black line, there are unipolar boundary layers between like-polarity open field regions. An example is the boundary layer between the open field regions with red and green colors and with green and dark blue colors.

Figures 2 and 3 show that as solar activity increases, the fraction of the solar surface occupied by even-numbered bipolar closed regions increases, as expected. Is the year-to-year variation in storm-effective solar wind structure associated with the solar cycle variation in the global distribution of the two kinds of closed field regions?

4. The central position of frontside full halo CMEs

The year-to-year variation in the storm-effectiveness of FFH CMEs may be associated with the solar cycle variation in the characteristics of the source regions of the FFH CMEs. Because CMEs are believed to be large-scale ejections of coronal plasma and magnetic field generated by free magnetic energy, their source regions are expected to involve large-scale closed field regions. It has been assumed that the bipolar helmet streamer, i.e., the closed field region sandwiched between two opposite-polarity open field regions, is the primary source region of CMEs (Hundhausen, 1993), at least during the phase near solar minimum. It was shown recently that the unipolar helmet streamer is the source of a considerable number of limb CMEs with smaller values of the velocity, mass, size and kinetic energy at solar activity maximum (Fainshtein, 1997; Eselevich et al., 1999).

Figures 4a and 4b display the candidate source location of 80 FFH CMEs between Jan. 1997 and Dec. 2000 on 80 Carrington synoptic maps of large-scale closed field regions that are sandwiched between open field regions. The Carrington rotation number and the date (YYYYMMDD) and time (UT) of the onset of FFH CMEs are shown at top of each map. For the 'too close' CMEs mentioned in Section 2, the Carrington rotation number on the top of each panel is replaced by the phrase 'Too Close CME'. The blue and red areas denote, as in Figure 2, the positive and negative open field regions computed using observations of the photospheric magnetic field at the Wilcox Solar Observatory and the potential field source surface coronal field model with the source surface located at 2.5 solar radii. The areas between the open field regions, both opposite- and like-polarity, denote large-scale closed field regions. The closed field regions between two opposite-polarity open field regions correspond to the bipolar coronal helmet streamers. The closed field regions between two like-polarity open field regions correspond to the unipolar helmet streamers. The black curve in each panel is the source surface neutral line at 2.5 R_S, denoting the bipolar streamer belt. As

the solar activity increases from near sunspot minimum to maximum, the inclination (i.e., tilt) of the neutral line increases from nearly parallel to nearly perpendicular to the solar equator (Hoeksema, 1991).

It is generally assumed that the source regions of CMEs are associated with solar surface activity such as flares (and their associated active regions) and filament disappearances. The surface locations of flares and filament disappearances associated with CMEs are usually offset from the axis of the CME (Harrison, 1986; Webb, 1992; Plunkett et al., 2001). The central position angle of a CME near the solar limb is usually defined to lie midway between the outer edges of the CME in a coronagraph image. For a symmetrical full halo CME, its central position is expected to be located near both the Sun's disk center and any associated surface activity (Zhao et al., 2001b). The symbol '+' in each panel of Figures 4a and 4b denote the Sun's disk center, i.e., the sub-Earth point, at the onset time of each FFH CME, given at the top of each panel. The symbols '$*$' and 'x' denote the associated solar surface activity located, respectively, within and greater than 45° of the Sun's disk center. The red, green and dark colors for symbols '+', '$*$' and 'x' indicate that the event is storm-associated, non-storm-associated, and indeterminate, respectively (see Table 2).

Table 2. The meaning of color symbols in Figures 4a and 4b

	Sun's disk center at onset of CME	Surface Activity within 45° of disk center	Surface Activity greater than 45° of disk center
Storm-associated	red +	red $*$	red x
Non-storm-associated	green +	green $*$	green x
Storm-association indeterminate	dark +	dark $*$	dark x

Figures 4a and 4b show that most of the locations of the surface activity associated with FFH CMEs appear to occur at or near the bipolar streamer belt, suggesting that they originate in bipolar helmet streamers. To quantify this, we connect the locations of the surface activities associated with the FFH CMEs ('$*$' or 'x') and the Sun's disk

centers ('+') with straight lines. We then consider a CME to be associated with the neutral line and, thus, originating in a bipolar helmet streamer, if this line crosses or is within $\pm$ 15° of the source surface neutral line. This width range was chosen to approximate the typical width of a bipolar helmet streamer (e.g., Hundhausen, 1993). Figures 4a and 4b indicate that there are 58 events which satisfied this criterion. However, LASCO observed some limb CMEs that begin near the inner edge of the helmet and show clear non-radial motion in the first few solar radii (Plunkett et al., 1997), suggesting that their associated surface activity may be displaced from the coronal streamer belt. For the remaining 22 events, we need to determine whether the connected line is located between two 'opposite-polarity' or two 'like-polarity' open field regions. We found that 8 events were located within bipolar helmet streamers, 3 within unipolar helmet streamers, and 11 were indeterminate. Thus, at least 83% of the FFH CMEs likely originated in bipolar helmet streamers. Observational evidence shows that the magnetic field topology of FFH CMEs can be assumed to be flux ropes (Webb, 2002). The internal field of magnetic flux ropes can be characterized by both axial and transverse components. The major component is the axial one near the rope center and the transverse component toward the rope's outer edge. At intermediate distances from the axis the field lines are helices with increasingly steeper pitch and decreasing field strength away from the axis of the rope. Depending on the orientation of the flux rope, both components of the internal field can contribute to the southward component of the IMF (Zhao et al., 2001a). If the rope is oriented west-east, the major contributor to Bs events is the transverse component of the internal field; and if the rope is oriented north-south the axial component dominates. The orientation of flux ropes can be determined by the inclination, with respect to the solar equator, of the associated neutral line or coronal streamer belt (Zhao and Hoeksema, 1996).

We can use these data to better understand the magnetic geometry of the source regions of FFH CMEs as a function of their geoeffectiveness. For this purpose we

exclude the 10 events that were too close together in time to distinguish separate storms at Earth. There are 45 storm-associated, 23 non-storm-associated and 2 association-indeterminate FFH CMEs indicated by red, green and dark '$*$' or 'x', respectively. Of the 24 events in 1997 and 1998, when most of closed field regions were bipolar helmet streamers and the neutral lines had low inclinations, 23 were located within bipolar streamers and near the neutral line, and only one was indeterminate for its source region. All 5 non-storm-associated FFH CMEs in the period were located far from the Sun's disk center and marked by a green 'x' (see Figure 4a). This suggests that the inclination of the associated segments of the coronal streamer belt for these events are rather low, suggesting the flux ropes are basically west-east oriented. Thus, these CMEs are located far from Sun's disk center so that a spacecraft near Earth might only penetrate the outermost, lower or upper part of the flux ropes where the internal field is basically parallel to the ecliptic plane. In 1999 and 2000, among 17 non-storm-associated FFH CMEs, the central positions of 14 originated in bipolar streamers, 2 in unipolar streamers and 1 was indeterminate. 11 of these 14 FFH CMEs originated in bipolar streamers located near those portions of the neutral line that had high local inclinations, and the other 3 with neutral lines with low inclinations. For the three events near the neutral line with low inclination, i.e., onsets at 19990622_18:54, 19990624_13:31 and 20000707_10:26 (see Figures 4a and 4b), the associated surface activity of the first two occurred greater than 30° from disk center; the portion of the neutral line near the third event was located at high latitude. Thus, except for these few cases, the central positions of the non-storm-associated FFH CMEs were located near those portions of the neutral line that had high local inclinations.

Figures 4a and 4b show that multiple FFH CMEs can occur in the same helmet streamer. For example, events 20000606_15:30, 20000607_16:30 in CR1963, and events 20000711_13:27, 20000714_10:53 and 20000809_16:30 in CR1965 and CR1966. (see Figures 4a and 4b). Among 33 FFH CMEs in 2000, there are at lease 10 storm-effective

FFH CMEs (with red '$*$' and + in Figures 4a and 4b) that occurred in four bipolar helmet streamers. If these 10 events would have occurred in 10 different helmet streamers, then only four events were probably storm-effective assuming that the probability for helmet streamer to generate storm-effective FFH CME in 2000 is the same as that in 1999. In this way, the fraction of storm-effective FFH CMEs to all FFH CMEs in 2000 becomes 52%. Thus, in 2000 compared to 1999 more FFH CMEs clustered in just a few low-heliolatitude bipolar helmet streamers; this is a major reason why the fraction of storm-associated to all FFH CMEs was higher in 2000 than in 1999.

5. Summary and discussion

Observations of FFH CMEs and their associated solar surface activity, interplanetary disturbances and geomagnetic storms during the first half of cycle 23 reveal the existence of a solar cycle trend in the storm-effectiveness of FFH CMEs. Nearly all FFH CMEs during the early ascending phase of solar cycle 23 were associated with geomagnetic storms, but only about 40% of them in 1999 could be linked with storms. The clustering in four low-heliolatitude large-scale closed field regions of many of the storm-associated FFH CMEs in 2000 is a major factor that caused the storm-effectiveness of FFH CMEs in 2000 to increase compared to 1999.

We find that most of the central positions of the FFH CMEs from 1997 to 2000 were located under the bipolar coronal streamer belt, suggesting that bipolar coronal helmet streamers are the primary source regions of CMEs (also supported in solar wind data by Kahler et al., 1999). Webb et al. [The Characteristics and Associations of Full Halo CMEs; Journal of Geophysical Research; in preparation, 2002] conclude that only CMEs which are faster and denser than average can be detected by LASCO as full halos. This result is consistent with the origins of halo CMEs being in bipolar helmet streamers, because some of the most massive, if not energetic CMEs have been observed to be blowouts of preexisting bipolar streamers (e.g., Hundhausen, 1999; Plunkett et.

al., 2000).

All six of the frontside halo CMEs from December 1996 to June 1997 had the magnetic field configuration of a flux rope as mentioned before. The 3-D shell or bubble model that is used to interpret the formation of the halo CMEs is actually implicit in the characterization of mass ejections as disruptions of an arcade of closed field lines (a cavity) above a polarity reversal line (usually a prominence) [Low and Hundhausen, 1995; Hundhausen, 1999]. This implies that all full halo CMEs contain a magnetic flux rope. To the contrary if some CMEs originate in unipolar streamers, their magnetic configurations might be complex and not contain 'simple' flux ropes, so they might not appear as halo CMEs when erupting near disk center.

The heliospheric current sheet, the boundary layer between open field regions having opposite magnetic polarity, has been suggested as the conduit for the propagation of flux rope-like CMEs (Crooker et al., 1993; Zhao and Hoeksema, 1996). Our conclusion that the central position of frontside full halo CMEs typically lies near the heliospheric current sheet confirms this suggestion. The heliospheric current sheet is basically aligned with underlying filaments in the corona and with the orientation of magnetic clouds (ICMEs) near the Earth (Zhao and Hoeksema, 1996; Mulligan et al., 1998; Webb et al., 2001). The solar cycle evolution of the neutral line thus implies that FFH CMEs or magnetic flux ropes near sunspot minimum are typically west-east oriented, and near sunspot maximum north-south oriented. The orientation of magnetic clouds has been shown to be a major factor that determines the duration and intensity of southward interplanetary magnetic field (Zhao and Hoeksema, 1998; Zhao et al., 2001a). Thus, the observation that halo CMEs, or their flux ropes, oriented west-east (north-south) near activity minimum (maximum) suggests that frontside full halo CMEs near minimum (maximum) have a stronger (weaker) chance of generating southward IMF events at 1 AU and, therefore, geomagnetic storms. This explanation for the lower storm-effectiveness of FFH CMEs near activity maximum is supported by earlier

observations near the maximum of cycle 21 during 1978-1979 that most fast CMEs that struck the magnetosphere did not produce intense storms, because they did not have sustained periods of strong southward field (Tsurutani et al., 1988). Thus, the close relationship of FFH CMEs to their solar origins in the streamer belt at the base of the heliospheric current sheet may be the major cause of the solar cycle evolution in their geoeffectiveness.

We caution, however, that other causes, such as the propagation speed of halo CMEs, may also affect their geoeffectiveness over the solar cycle (see Webb, 2002). The occurrence rate of CMEs increases from minimum to maximum by an order of magnitude, leading to multiple CMEs per day over the Sun or even from a single region (these in fact can confuse halo CME identifications.) Gopalswamy et al. (2001) have found since early 1998 several tens of LASCO CMEs wherein a faster CME overtakes a slower one within 30 R_S of the Sun, producing an interaction. Reconnection or sandwiching of each CME's field lines are likely in such cases. The combination of sequential eruptions of CMEs and their subsequent interactions can produce complex ejecta at 1 AU. Such ejecta often consist of high speed flows with shocks and other ICME signatures, but poorly defined magnetic structures with, for example, little coherent southward field (Burlaga et al., 2001). In addition, the rate at which CMEs actually encounter Earth near maximum is modified by their broadening latitude distribution (e.g., Hundhausen, 1993; St. Cyr et al., 2000). Thus, although the CME rate is considerably higher at maximum, proportionally fewer CMEs are ejected near the ecliptic plane because of the highly tilted streamer belt and broadening latitude distribution. Finally, the "background" solar wind into which the CMEs are injected is itself much more complex near maximum. This creates more frequent and complicated interactions of ejecta with the existing structure, leading to distortions and compressions which are difficult to simulate and predict (e.g., Odstrcil and Pizzo, 1999). All these factors may contribute to the changing degree of storm-effectiveness of frontside full

halo CMEs over the solar cycle, and some may help explain why the storm-effectiveness of frontside full halo CMEs near sunspot maximum is relatively low.

6. Acknowledgements

We benefitted from data from the SOHO mission, which is an international collaboration between NASA and ESA, from the Kitt Peak National Observatory Internet site, and from the SOHO/ LASCO CME catalog, generated and maintained by the Center for Solar Physics and Space Weather, The Catholic University of America in cooperation with the Naval Research Laboratory and NASA. We are grateful to E. Cliver and S. Kahler for helpful comments. X. P. Zhao was supported at Stanford University by NASA grants NAGW 2502 and NAG5-3077, by NSF grant ATM9400298, and by ONR grant N0014-97-1-0129, and D. Webb was supported at Boston College by Air Force contract AF19628-00-K-0073 and NASA grant NAG5-10833.

References

Bothmer, V. and D. M. Rust, The field configuration of magnetic clouds and the solar cycle, in *Coronal Mass Ejections, Geophys. Monogr. Ser.,* vol. 99, edited by N. Crooker et al., p. 139, AGU, Washington, D.C., 1997.

Brueckner, G. E., et al., The large-angle spectroscopic coronagraph (LASCO), *Solar Phys.*, 162, 357, 1995.

Burlaga L.F., R.M. Skoug, C.W. Smith, D.F. Webb, T.H. Zurbuchen and A. Reinard, Fast ejecta during the ascending phase of solar cycle 23: ACE observations, 1998-1999, *J. Geophys. Res.*, 106, 20,957, 2001.

Cane, H.V., I.G. Richardson, and O.C. St. Cyr, Coronal mass ejections, interplanetary ejecta and geomagnetic storms, *Geophys. Res. Lett.,* 27, 3591, 2000.

Crooker, N.U., Siscoe, G.L., Shodhan, S., Webb, D.F., Gosling, J.T., and E.J. Smith, Heliospheric Current Sheets and Coronal Streamer Belt Dynamics, *J. Geophys. Res.*, 98,. 9371, 1993.

Eselevich, V.G., On the structure of coronal streamer belts, *J. Geophys. Res.*, 103, 2221, 1998.

Eselevich, V.G., V.G. Fainshtein and G.V. Rudenko, Study of the structure of streamer belts and chains in the solar corona, *Solar Phys., 188*, 277, 1999.

Fainshtein V.G., An investigation of solar factors governing coronal mass ejections characteristics, *Solar Phys., 174*, 413, 1997.

Gopalswamy, N., S. Yashiro, M.L. Kaiser, R.A. Howard, and J.L. Bougeret, Radio signatures of coronal mass ejection interaction: coronal mass ejection cannibalism? *Astrophys. J.*, 548, L91, 2001.

Gosling, J. T., et al., Geomagnetic activity associated with earth passage of interplanetary shock disturbances and coronal mass ejections, *J. Geophys. Res., 96*, 7831, 1991.

Harrison, R. A., Solar coronal mass ejections and flares, *Astron. Astrophys., 162*, 283,

1986.

Hoeksema, J. T., Large-scale structure of the heliospheric magnetic field: 1976-1991, *Adv. Space Res., 9*, 15, 1991.

Howard, R. A., D. J. Michels, N. R. Sheeley, Jr., and M. J. Koomen, The observation of a coronal transient directed at Earth, *Astrophys. J.*, 263, L101, 1982.

Howard, R.A., Sheeley, N.R. Jr., Koomen, M.J., and Michels, D.J., Coronal mass ejections: 1979-1981, *J. Geophys. Res.*, 90, 8173, 1985.

Hundhausen, A. J., Coronal expansion and solar wind, *Physics and Chemistry in Space, Vol. 5,* Springer-Verlag, New York, 1972.

Hundhausen, A. J., Size and locations of coronal mass ejections: SMM observations from 1980 and 1984 – 1989, *J. Geophys. Res., 98*, 13177, 1993.

Hundhausen, A. J., A summary of SMM observations from 1980 and 1984-1989, in *The Many Faces of the Sun: Scientific Highlights of the Solar Maximum Mission*, edited by K. T. Strong, J. L. R. Saba, B. M. Haich and J. T. Schmelz, Springer-Verlag, New York, p. 143, 1999.

Kahler, S. W., Solar flares and coronal mass ejections, *Ann. Rev. Astron. Astrophys.*, 30, 113, 1992.

Kahler, S. W., N.U. Crooker, and J.T. Gosling, The polarities and locations of interplanetary coronal mass ejections in large interplanetary magnetic sectors, *J. Geophys. Res., 104*, 9919, 1999.

Low, B.C. and J.R. Hundhausen, Magnetostatic structures of the solar corona. II. The magnetic topology of quiescent prominences, *Astrophys. J*, 443, 818, 1995.

Mulligan, T., C. T. Russell, and J. G. Luhmann, Solar cycle evolution of the structure of magnetic clouds in the inner heliosphere, *Geophys. Res. Lett., 25*, 2959, 1998.

Neugebauer, M. and R. Goldstein, Particle and field signatures of coronal mass ejections in the solar wind, in *Coronal Mass Ejections*, Geophysical Monograph Vol. 99, edited by N. Crooker et al., p. 245, Washington, DC., 1997.

Odstrcil, D., and V. J. Pizzo, Distortion of the interplanetary magnetic field by three-dimensional propagation of coronal mass ejections in a structured solar wind, *J. Geophys. Res.*, 104, 28,225, 1999.

Plunkett, S. P., et al., The relationship of green-line transients to white-light coronal mass ejections, *Solar Phys., 175*, 699, 1997.

Plunkett, S.P. et al., Simultaneous SOHO and Ground-based observations of a large eruptive prominence and coronal mass ejection, *Solar Phys.*, 194, 371, 2000.

Plunkett, S. P., et al., Solar source regions of coronal mass ejections and their geomagnetic effects, *J. Atmos. Sol.-Terres. Phys., 63*, 389, 2001.

Saito, K. And E. Tandberg-Hanssen, The arch systems, cavities and prominences in the helmet streamer observed at the solar eclipse, November 12, 1966, *Solar Phys.*, 31, 105, 1973.

Schwenn, R. et al., First view of the extended green-line emission corona at solar activity minimum using the LASCO-C1 coronagraph on SOHO, *Solar Phys.*, 175, 667, 1997.

Solar Geophysical Data Bulletins, NOAA Natl. Geophysical Data Center, WDC-A, Boulder, Colo., 2002.

St. Cyr, O.C., et al., Properties of coronal mass ejections: SOHO LASCO observations from January 1996 to June 1998, *J. Geophys. Res., 105*, 18169, 2000.

Thompson, B. J., et al. SOHO/EIT observations of an Earth-directed coronal mass ejection on May 12, 1997, *Geophys. Res. Lett., 25*, 2461, 1998.

Tsurutani, B.T., and W.D. Gonzales, The interplanetary causes of magnetic storms: A review, in *Magnetic Storms,* GM 98, p. 77, American Geophysical Union, Washington, D.C., 1997.

Tsurutani, B. T., et al., Comment on 'A new method of forecasting geomagnetic activity and proton showers' *Planet. Space Sci., 36*, 205, 1988.

Wang, Y.-M., N. R. Sheeley, Jr., and N. B. Rich, Evolution of coronal streamer structure

during the rising phase of solar cycle 23, *Geophys. Res. Lett., 27*, 149, 2000.

Webb, D.F., The Solar Sources of Coronal Mass Ejections, in (Z. Svestka, B.V. . Jackson and M.E. Machado, eds.) *Eruptive Solar Flares*, Springer-Verlag, Berlin, Heidelberg, p. 234, 1992.

Webb, D.F., CMEs and the solar cycle variation in their geoeffectiveness, in *From Solar Min to Max; Proceedings of the SOHO-11 Symposium*, SP-508, p. 409, ESA, ESTEC, Noordwijk, The Netherlands, 2002.

Webb, D.F., S.W. Kahler, P.S. McIntosh, and J.A. Klimchuk, Large-scale structures and multiple neutral lines associated with CMEs, *J. Geophys. Res.*, 102, 24,161, 1997.

Webb, D. F., E.W. Cliver, N.U. Crooker, O.C. St. Cyr and B.J. Thompson, Relationship of halo coronal mass ejections, magnetic clouds, and magnetic storms, *J. Geophys. Res., 105*, 7491, 2000.

Webb, D. F., N. U. Crooker, S. P. Plunkett, and O. C. St. Cyr, The solar source of geoeffective structures, in *Space Weather*, AGU Geophysical Monograph 125, edited by P. Song, G. Siscoe, and H. Singer, p. 123, 2001.

Zhao, X. P. and J. T. Hoeksema, Effect of coronal mass ejections on the structure of the heliospheric current sheet, *J. Geophys. Res., 101*, 4825, 1996.

Zhao, X. P. and J. T. Hoeksema, Central axial field direction in magnetic clouds and its relation to southward interplanetary magnetic field events and dependence on disappearing solar filaments, *J. Geophys. Res., 103*, 2077, 1998.

Zhao, X.P., J.T. Hoeksema, J.T. Gosling, and J.L. Phillips, Statistics of IMF Bz events, in *Solar-Terrestrial Predictions - IV, Vol. 2,* edited. by J. Hruska et al., p. 712, NOAA, Boulder, Colo., 1993.

Zhao, X. P., J. T. Hoeksema and P. H. Scherrer, Changes of the boot-shaped coronal hole boundary during Whole Sun Month near sunspot minimum, *J. Geophys. Res., 104*, 9735, 1999.

Zhao, X. P., J. T. Hoeksema, and K. Marubashi, Magnetic cloud Bs events and their dependence on cloud parameters, *J. Geophys. Res., 106*, 15643, 2001a.

Zhao, X. P., S. Plunkett and W. Liu, The geometrical and kinematical properties of the 1997 May 12 halo coronal mass ejection, *J. Geophys. Res.*, In press, 2001b.

X. P. Zhao, W. W. Hansen Experimental Physics Laboratory, Stanford University, Stanford, CA 94305-4085. (e-mail: xpzhao@solar.stanford.edu)

D. F. Webb, AFRL/VSBXS, 29 Randolph Road, Hanscom AFB, MA 01731-3010. (e-mail: david.webb@hanscom.af.mil)

Received _____

Version: 11 November 2002

Figure 1. A sketch of the solar corona observed at the November 12, 1966 eclipse. The twin arch system and an overlying helmet streamer are seen in the NW quadrant. Quiescent prominences seen as dark filaments are shown on the disk (Courtesy to Kuniji Saito for copying).

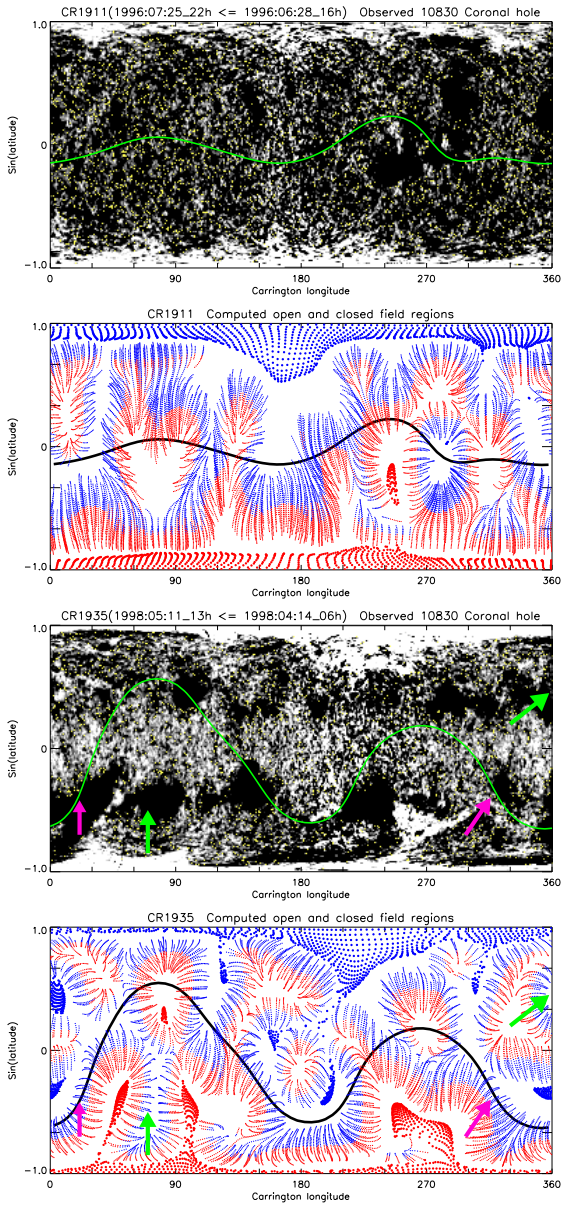

Figure 2. Panels 1 and 3: Carrington synoptic HeI 10830$\mathring{A}$ maps. The large white and dark areas denote coronal holes and active regions, respectively. Panels 2 and 4: The computed coronal open (red and blue dot area) and closed (areas consisting of field lines made by blue [upward] and red [downward] segments) field regions are shown. The green and purple arrows in the bottom panel denote the two kinds of closed field regions discussed in the text. The thick black or green curve marks the magnetic neutral line, representative of the coronal streamer belt at the base of the heliospheric current sheet.

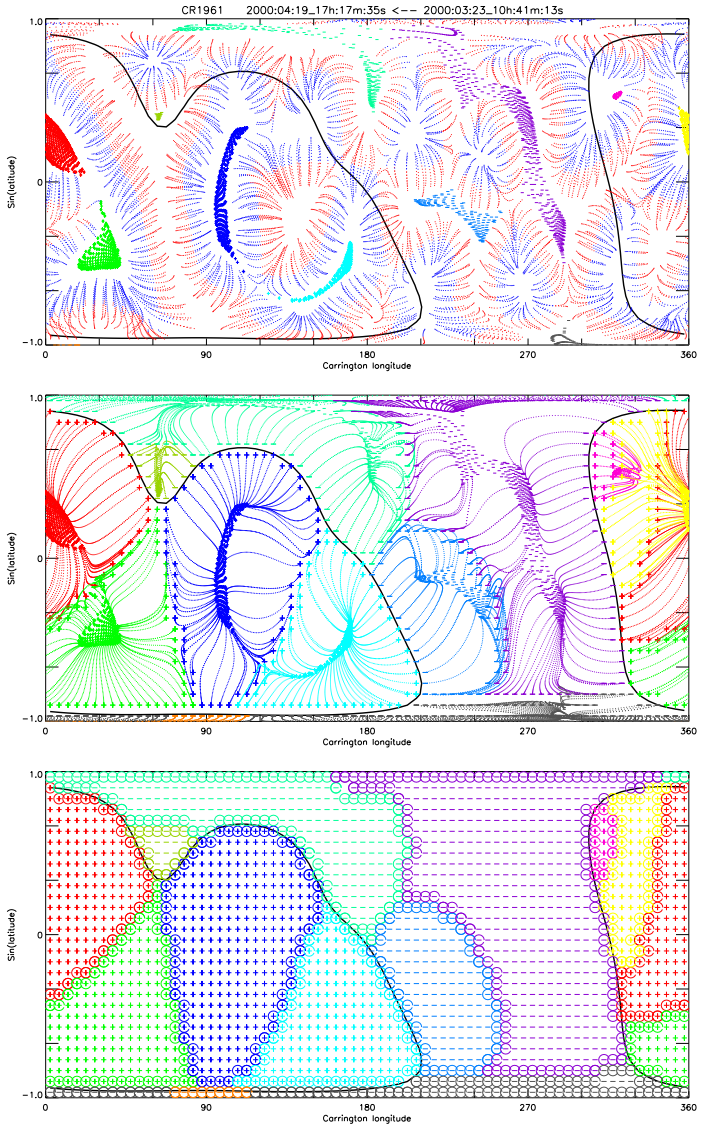

Figure 3. The coronal open (colored dot areas) and closed (the areas consisting of blue-red field lines) field regions below 1.25 R_S near maximum activity (CR1961) (top panel), the radial extension of the boundaries of open field regions to the source surface at 2.5 R_S (middle panel), and the two kinds of boundary layers between open field regions at the source surface: bipolar (coincident with the black neutral line) and unipolar boundary layers (bottom panel).

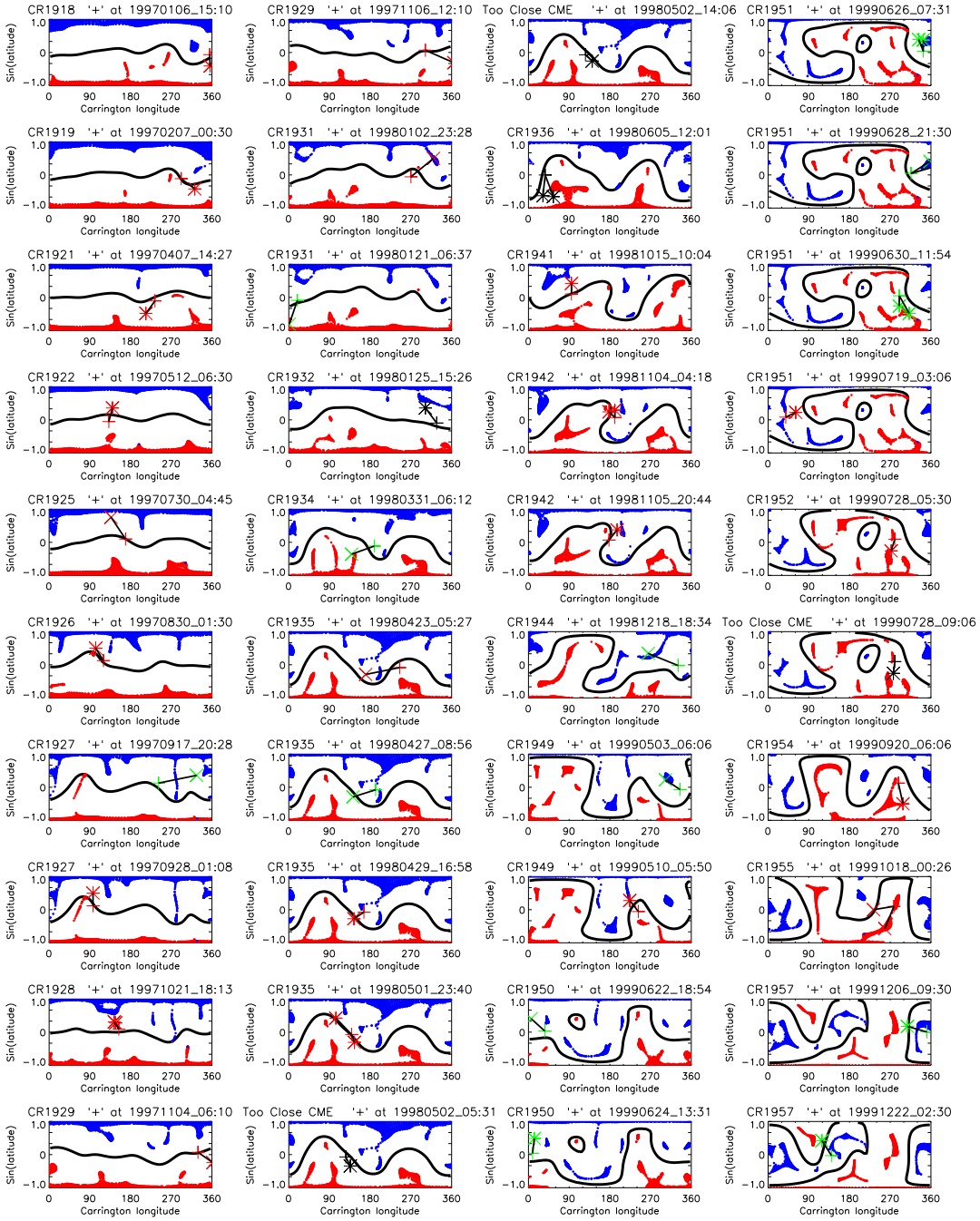

Figure 4a. The candidate source location ('+', '∗' and 'x') of the 40 FFH CMEs between Jan. 1997 and Dec. 1999 placed on the appropriate Carrington synoptic maps of large-scale closed field regions. The the Carrington rotation number and the date and time of the onset of FFH CMEs are shown at the top of each map. (See paragraphs 2 and 3 of Section 4 and Table 2 for the details).

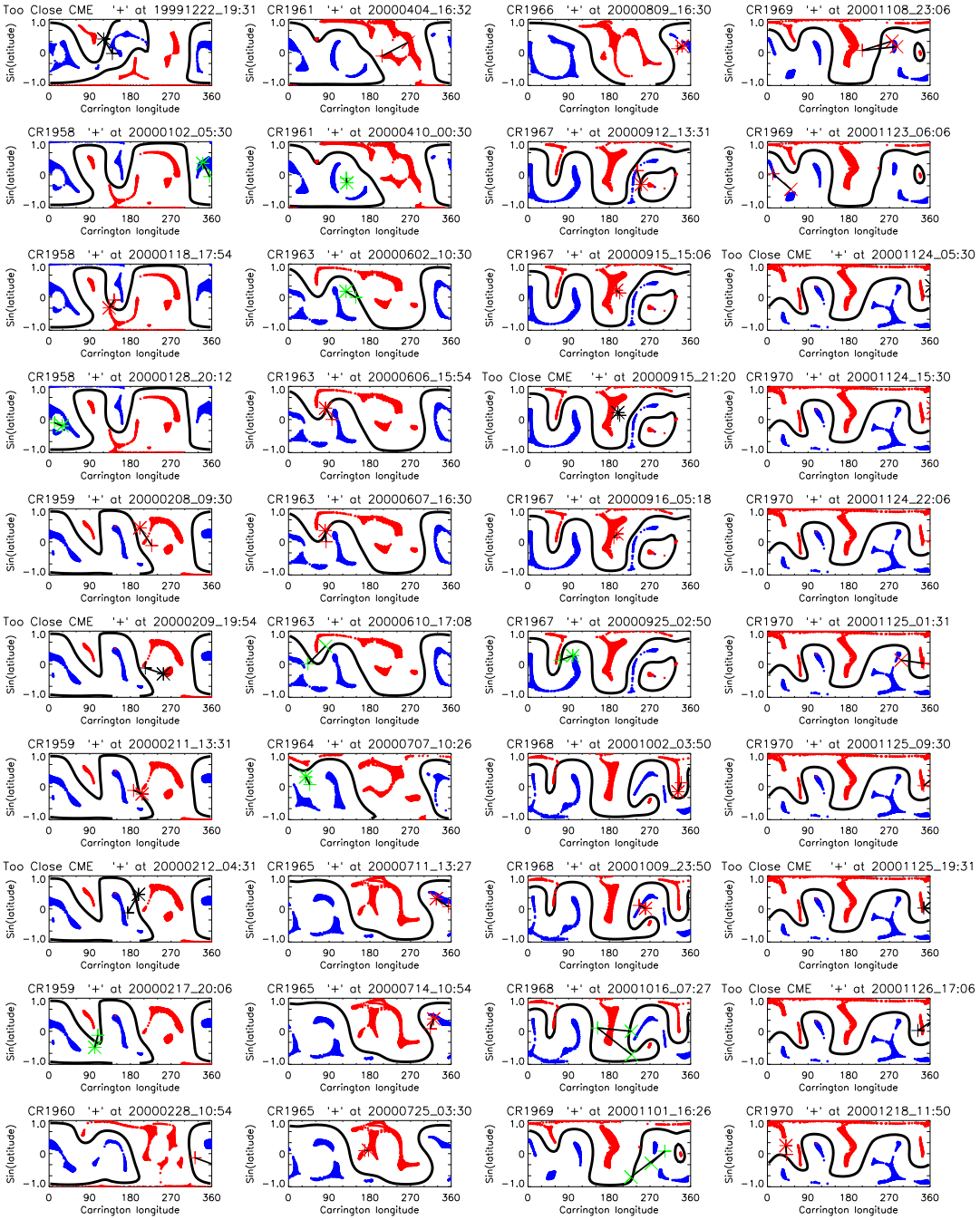

Figure 4b. The same as Figure 4a but between Dec. 1999 and Dec. 2000.